The Role of Surface Oxygen Vacancies in the NO 2 Sensing Properties of SnO 2 Nanocrystals

ARTICLE *in* THE JOURNAL OF PHYSICAL CHEMISTRY C · DECEMBER 2008

Impact Factor: 4.77 · DOI: 10.1021/jp804916g

11 AUTHORS, INCLUDING:

Mauro Epifani
Italian National Research Council
101 PUBLICATIONS **1,686** CITATIONS
SEE PROFILE

Elisabetta Comini
Università degli Studi di Brescia
359 PUBLICATIONS **7,915** CITATIONS
SEE PROFILE

Maurizio Avella
Italian National Research Council
244 PUBLICATIONS **3,806** CITATIONS
SEE PROFILE

Franca Morazzoni
Università degli Studi di Milano-Bicocca
119 PUBLICATIONS **2,283** CITATIONS
SEE PROFILE

Article

The Role of Surface Oxygen Vacancies in the NO Sensing Properties of SnO Nanocrystals

Mauro Epifani, Joan Daniel Prades, Elisabetta Comini, Eva Pellicer, Manuel Avella, Pietro Siciliano, Guido Faglia, Albert Cirera, Roberto Scotti, Franca Morazzoni, and Joan Ramon Morante

J. Phys. Chem. C, **2008**, 112 (49), 19540-19546 • Publication Date (Web): 14 November 2008

The Role of Surface Oxygen Vacancies in the NO_2 Sensing Properties of SnO_2 Nanocrystals

Mauro Epifani,*,† Joan Daniel Prades,‡ Elisabetta Comini,§ Eva Pellicer,‡ Manuel Avella,‖ Pietro Siciliano,† Guido Faglia,§ Albert Cirera,‡ Roberto Scotti,⊥ Franca Morazzoni,⊥ and Joan Ramon Morante‡

Consiglio Nazionale delle Ricerche, Istituto per la Microelettronica ed i Microsistemi (C.N.R.-I.M.M.), via Monteroni, I-73100 Lecce, Italy, EME/XaRMAE/IN²UB, Departament d'Electrònica, Universitat de Barcelona, C.\ Martí i Franquès 1, E-08028 Barcelona, Spain, CNR-INFM and Dipartimento di Chimica e Fisica per l'Ingegneria e i Materiali, SENSOR, Università di Brescia, via Valotti 9, Brescia, Italy, Departamento de Física de la Materia Condensada, Universidad de Valladolid, Paseo del Prado de la Magdalena, Valladolid, Spain, and Dipartimento di Scienza dei Materiali, Università degli Studi di Milano-Bicocca, via R. Cozzi 53, 20125 Milano, Italy

Received: June 4, 2008; Revised Manuscript Received: September 30, 2008

SnO_2 nanocrystals were prepared by injecting a hydrolyzed methanol solution of $SnCl_4$ into a tetradecene solution of dodecylamine. The resulting materials were annealed at 500 °C, providing 6−8 nm nanocrystals. The latter were used for fabricating NO_2 gas sensing devices, which displayed remarkable electrical responses to as low as 100 ppb NO_2 concentration. The nanocrystals were characterized by conductometric measurements, X-ray photoelectron spectroscopy (XPS), electron paramagnetic resonance (EPR), and cathodoluminescence (CL) spectroscopy. The results, interpreted by means of molecular modeling in the frame of the density functional theory (DFT), indicated that the nanocrystals contain topographically well-defined surface oxygen vacancies. The chemisorption properties of these vacancies, studied by DFT modeling of the NO_2/SnO_2 interaction, suggested that the in-plane vacancies facilitate the NO_2 adsorption at low operating temperatures, while the bridging vacancies, generated by heat treatment at 500 °C, enhance the charge transfer from the surface to the adsorbate. The behavior of the oxygen vacancies in the adsorption properties revealed a gas response mechanism in oxide nanocrystals more complex than the size dependence alone. In particular, the nanocrystals surface must be characterized by enhanced transducing properties for obtaining relevant gas responses.

Introduction

The use of semiconducting metal oxide (MOX) nanocrystals was suggested at the beginning of the 90's by Yamazoe and co-workers[1] as a powerful way for improving the performances of chemoresistive gas-sensors. The high response of nanocrystal-based sensors was predicted and experimentally demonstrated by the same authors. They explained the sensitivity in terms of enhanced modulation of the charge depletion layer due to the interaction with the surrounding gases. Since then, intensive efforts were devoted to the development of metal oxide nanostructure-based gas-sensors, and an increasing number of papers appeared in the literature. This fact confirms the potential of nanosized metal oxides in gas-sensing applications, either as 0-D nanocrystals[2] or as 1-D nanostructures,[3] such as nanobelts and nanowires. In a recent work,[4] we developed a wet chemical synthetic route for the preparation of metal oxide nanocrystals (mainly SnO_2, In_2O_3, Pd-SnO_2) employed as base materials for chemoresistive sensors.[5] Remarkable performances toward a broad range of gaseous analytes were obtained, which in the following will be focused on the SnO_2 sensing response toward NO_2, significantly high at low temperatures (25−100 °C). Thus we obtained a direct confirmation of the potential of nanosized oxides for improved gas sensors. On the other hand, when comparing our results with other literature reports, it appeared that the sensing properties span a very broad range, depending on the processing route, the thermal history, morphology of the material, and so on. This spread in the results cannot be fully explained by the dependence of the gas response on the particle size. It could be indeed a rough approximation to consider the nanometric size as a tool to improve the sensing properties, totally skipping the nature of the surface adsorption processes. This difficulty explicitly appears by referring to the classical expressions for the charge depletion depth w formed in the oxide grain upon gas adsorption:[6]

$$w = L_D(2\beta V_S)^{1/2} \quad (1)$$

where L_D is the Debye length, V_s the surface potential barrier, and $\beta = q/kT$, where q is the electron charge, k the Boltzmann constant, and T the temperature. The interest for oxide nanocrystals in gas-sensing stems from the possibility of having w comparable to the grain size and hence large relative electrical resistance change upon exposure to the gases. As the V_S value depends on the charge density established upon interaction with the gas, the value of w, for a given material and grain size, could span a whole range, depending on the surface capability of adsorbing gaseous species. This fact has to be carefully considered to achieve a deeper insight into the diverse sensing results of metal oxide nanocrystals and to rationally design their use in sensing devices.

* E-mail: mauro.epifani@le.imm.cnr.it.
† Istituto per la Microelettronica ed i Microsistemi.
‡ Universitat de Barcelona.
§ Università di Brescia.
‖ Universidad de Valladolid.
⊥ Università degli Studi di Milano-Bicocca.

10.1021/jp804916g CCC: $40.75
Published on Web 11/14/2008

It is generally proposed[6] that the NO_2 sensing at low operating temperatures, where we have obtained the highest responses, is due to NO_2 chemisorption and to the consequent charge depletion of the sensing material following the reaction:

$$NO_2(g) + e^- \leftrightarrow NO_2^-(ads) \quad (2)$$

Thus the case of NO_2 is particularly amenable to the study of the adsorption properties of the sensing materials. The aim of this work is just to demonstrate the relevance of the surface oxygen vacancies in NO_2 adsorption on nanocrystalline SnO_2 and in the related sensing properties. First of all, the chemical nature of the nanocrystal surface was established by conductometric measurements, XPS, EPR, CL spectroscopy, and DFT modeling. The presence of a strongly reduced surface was evidenced, characterized by very well topographically defined oxygen vacancies. The latter were used as an input in the ab initio DFT modeling of the SnO_2/NO_2 interaction. It was observed that the calculated adsorption energy and the charge transfer to adsorbed NO_2 were strongly enhanced by such oxygen vacancies. Since the NO_2-sensing mechanism is based onto the gas adsorption on the nanocrystals surface and the related charge transfer phenomena,[6] direct correlation between the NO_2 response and the surface oxygen vacancies could be established. It was concluded that the nanometer size regime may be not sufficient by itself to justify high gas response, if not coupled with well defined surface reception properties.

Experimental Section

SnO_2 nanocrystals were prepared by a general procedure based on the injection of metal oxide sols into a hot (160 °C) solution of dodecylamine in tetradecene, as fully described in previous work.[4] After 3 h from the injection step, the nanocrystals were extracted from the synthesis pot and dried at 80 °C. Then, they were heat-treated up to 500 °C in synthetic air in order to eliminate the organic residuals. After the heat treatment, the size of nanocrystals did not increase substantially, reaching the final value of about 6 nm.

The substrates for the processing of sensing devices were precut alumina plates (2×2 mm^2) onto whose back and front were deposited platinum heaters and titanium/platinum electrodes, respectively, by lithographic techniques. Powder suspensions were prepared by dispersing 4−6 mg of the heat-treated nanocrystals in 1−1.5 mL of methanol. Drops of the suspensions (about 4 μL) were deposited onto the substrates, waiting for complete evaporation of the solvent before depositing the next drop. Gold wires were bonded to the electrodes and heaters before the drop-coating step.

The flow-through technique was used to test the electrical properties of the thin films. A constant flux of synthetic air of 0.5 L/min was used as gas carrier. All the measurements were carried out in a temperature-stabilized sealed chamber at 20 °C under controlled humidity. The operating temperatures of the sensors were varied between 25 and 300 °C using the platinum heating meander integrated in the alumina substrate. The conductance was studied as a function of operating temperature and oxygen concentration using certified bottles with oxygen diluted in nitrogen. Electrical characterization was carried out by volt-amperometric technique at constant voltage, equal to 1 V, measuring the current through a picoammeter.

XPS (X-ray photoelectron spectroscopy) data were collected with a Physical Electronics 5500 spectrometer at a pressure of 6×10^{-9} Torr. Aluminum Kα X-rays were produced with an energy of 1486.6 eV and natural line width of 0.9 eV. All the spectra were fitted to reach the right carbon position (284.5 eV). The spectra were fitted with Gaussian−Lorentzian functions (80−20% respectively) and considering a Shirley baseline. Analyses were done both before and after Ar-ion sputtering for 1 min.

The cathodoluminescence measurements were carried out in a Gatan XiCLone system attached to a JEOL JSM-820 scanning electron microscope. The collected luminescence was analyzed by a 300-line grating monochromator and was detected by a Peltier cooled CCD, with a spectral range from 200 to 1200 nm. The system is equipped with a cryostat that allows low temperature measurements. The measurements were carried out at liquid nitrogen temperature (∼80 K). The excitation beam conditions were 20 kV for accelerating voltage and ∼40 nA for beam current.

Electron paramagnetic resonance (EPR) spectra were recorded by using a conventional Bruker EMX spectrometer operating at the X band frequency and magnetic field modulation of 100 kHz, with a microwave power of 5 mW and a modulation amplitude of 10 or 3 G. The g values were calculated by comparison with diphenylpicrylhydrazyl (DPPH) ($g = 2.0036$). Powdered samples were put into a quartz apparatus suitable for both gas flow interaction and EPR measurements. CO was used as a probe molecule. The following gas treatment sequence was adopted: (1) SnO_2, previously heat-treated at 500 °C, as described before, was treated in dry air stream (30 cm^{3}min^{-1}) for 90 min at 400 °C; (2) CO(600 ppm)/Ar mixture was passed over SnO_2 (30 cm^{3}min^{-1}) for 30 min at the same temperature. After each thermal gas treatment, the samples were quenched at room temperature (in about 5 min), and EPR spectra were recorded at 113 K, under the same atmosphere.

The first-principles methodology used in the present work was based on density functional theory[7,8] (DFT) as implemented in the SIESTA code.[9,10] We used the generalized gradient approximation (GGA) for the exchange-correlation functional (PBE96)[11] and norm-conserving Troullier−Martins pseudopotentials.[12] Solutions of the Kohn−Sham equations were expanded as linear combinations of atomic pseudo wave functions of finite range. For all atomic species, double ζ plus polarization orbital basis-sets were used. Oxygen atoms were described by six valence electrons, nitrogen by five, and tin atoms by four plus the corresponding pseudopotential ion cores. To deal with surface stability and adsorption energy calculations, we modeled all surface geometries as three dimensionally periodic slab systems, generated from the relaxed SnO_2−cassiterite[13] bulk unit cell, composed of five $O(Sn_2O_2)O$ layers with a vacuum width of 12 Å between surfaces to avoid interaction between periodic images of the slabs.[14−16] This procedure was successfully used in previous work.[16−20] We set a real space mesh cutoff[9,10] of 250 Ry and a $5 \times 5 \times 1$ Monkhorst-Pack set[21] to obtain total energies converged within 5 meV per six-atom unit cell, which is suitable for this kind of calculation.[14−16] Under these conditions, forces over atoms converged to better than 0.004 eV/Å^2. We also considered spin polarization in the total energy computations and corrected the basis set superposition error[22] (BSSE) in the calculated adsorption energies. We introduced structural relaxations by means of conjugate gradient minimization of the energy, until the forces on all the atoms were smaller than 0.04 eV/Å^2. In the relaxation of the slabs, supercell dimensions were kept constant and, as proposed by some authors, no constraints were imposed to the atomic positions within the supercell. In the slab composed of five layers, the maximum displacement of the atoms in the middle layer was as small as 0.05 Å.

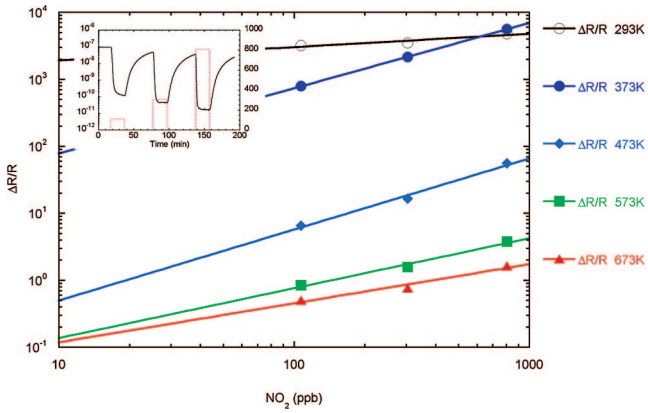

Figure 1. Calibration of SnO_2-based sensors to NO_2 at various operating temperatures. The inset shows a dynamic response curve measured at an operating temperature of 373 K.

Results

1. Review of NO_2 Sensing Properties. As shown in Figure 1, the main results concerning the NO_2 sensing properties of SnO_2 nanocrystals are the following[4,5] (we recall that the sensor response is defined as $(R_G - R_0)/R_0$, where R_G is the electrical resistance upon exposure to the gaseous analyte, and R_0 is the electrical resistance in pure synthetic air):

1. At 293 K, a huge response of more than 3 orders of magnitude was obtained toward as low as 100 ppb NO_2 concentrations.

2. At 373 K, the response decreased to about 3 orders of magnitude for the same concentration.

3. At 473 K, the response substantially dropped but still remained relatively high (about 70).

4. Beyond 473 K, the response decreases to values lower than unity.

2. The Chemical State of the Nanocrystals. ***(a) Conductance Measurements.*** Electrical characterization of the prepared nanomaterials was carried out by conductance measurements using different oxygen concentrations. These measurements were undertaken for characterizing the surface reactivity toward oxygen, since the oxygen adsorption is commonly invoked to explain the sensing mechanisms of metal oxides.[23] The results are reported in Figure 2 for SnO_2 nanocrystals heat-treated at 500 °C. At temperatures above 293 K, the increase in the oxygen concentration from 0 to 10% results in a remarkable conductance decrease.

The conductance drop is enhanced at higher temperatures, spanning a range of about 2 orders of magnitude. The current variation occurs upon injection of 10% O_2 and is more pronounced from 473 K. In this range of temperatures, ionosorption of atomic oxygen is known to be favored, while the adsorption of molecular oxygen is favored at lower temperatures.[23] We conclude that the surface reactions with ionosorbed oxygen control the electrical properties.

(b) Surface Chemical Composition by XPS. SnO_2 nanocrystals were analyzed by XPS both before and after Ar-ion sputtering. The survey spectra in Figure 2 show that they are chemically pure; even after sputtering no differences were seen in samples, except for the intensity of the C 1s signal. In fact, it is less than 0.5 atomic % after surface sputtering and confirms that the C presence is mainly due to adventitious surface contamination. The Cl moieties in SnO_2 nanocrystals disappear after the heat treatment at 500 °C. It is very important to observe that the O/Sn atomic ratio, obtained from the spectra analysis, is about 1.2, indicating a strongly reduced surface, if compared with the theoretical ratio of 2 for SnO_2. The reason for the strongly reduced sample stoichiometry was suggested in the previous description of the synthesis process.[4] It appeared that during the heat treatment a carbon layer is formed at the surface of the sample, so providing a strongly reducing environment. Figure 3

(c) EPR Assessment of the Surface Reduction. The reaction of gaseous analytes with SnO_2 can be monitored by EPR spectroscopy in terms of the subsequent formation of paramagnetic centers. It was demonstrated[24] that the reaction of CO follows the equations:

$$CO + O_O \leftrightarrow V_O + CO_2 \quad (3)$$

$$V_O \leftrightarrow V_O^{\bullet} + e^- \quad (4)$$

where V_O is a *shallow* neutral oxygen vacancy, O_O an oxide anion in a regular lattice site, and $V_O^{\bullet}$is a singly ionized, paramagnetic oxygen vacancy. EPR investigation was performed on nanocrystalline SnO_2 to detect the formation and the reactivity of such shallow defects, after thermal annealing and successive reaction with the gas. CO was used as a probe molecule, according to procedure reported in the Experimental Section, at 400 °C.

The sample heat-treated at 500 °C after the synthesis shows a very weak isotropic signal at $g = 1.91$ attributed to paramagnetic monoionized oxygen vacancies $V_O^{\bullet}$,[24] which do not change after further annealing in air at 400 °C (Figure 4a). After successive reaction with CO (600 ppm)/Ar at 400 °C, no new paramagnetic vacancies are formed (Figure 4b). These results do not follow the general trends observed in other work.[24] Residual $V_O^{\bullet}$, already present in the 500 °C heat-treated SnO_2 and after further treatment at 400 °C in air, are not reactive and are more likely located in the lattice far from the surface. The difficult formation of further paramagnetic species after treatment with CO at 400 °C is closely related to the peculiar surface chemistry evident in our samples. In particular, the absence of CO interaction with the sample surface is in agreement with the presence of a strongly reduced surface, as demonstrated by the electrical, XPS, CL, and simulation results: further reduction by CO is hindered for thermodynamic reasons, implying an energetically unlikely surface configuration.

(d) Investigation of the Surface Structure: Cathodoluminescence Measurements on the SnO_2 Nanocrystals. For investigating the surface states in low-conductive systems, cathodoluminescence (CL) is one of the best suited techniques.[17,18,25] It was shown in previous work[17] that the visible CL spectrum of SnO_2 is dominated by a broad signal composed of four different contributions centered around 1.90, 2.20, 2.37, and 2.75 eV (from now on I, II, III, and IV, respectively). On the basis of DFT calculations, these bands were assigned to radiative recombinations from the minimum of the conduction band and the SnO_2-intrinsic bulk shallow levels toward intragap states near the top of the valence band corresponding to surface oxygen vacancies. For the most common low index surfaces of SnO_2−cassiterite (namely (110), (100), (101), and (001)), the calculations revealed two families of states corresponding to two different angles between the oxygen site and the first neighboring tin atoms. Following the usual notation for the SnO_2(110)−cassiterite surface (which is the most stable, abundant, and deeply studied facet), the bands I and II were related to bridging oxygen vacancies ($O_{BridgVac}$) whereas the bands III and IV were attributed to in-plane oxygen vacancies ($O_{InPlaneVac}$). These results are summarized in Figure 5.

This model explained the CL spectra of a full set of SnO_2 nanomaterials obtained by different synthetic methods and

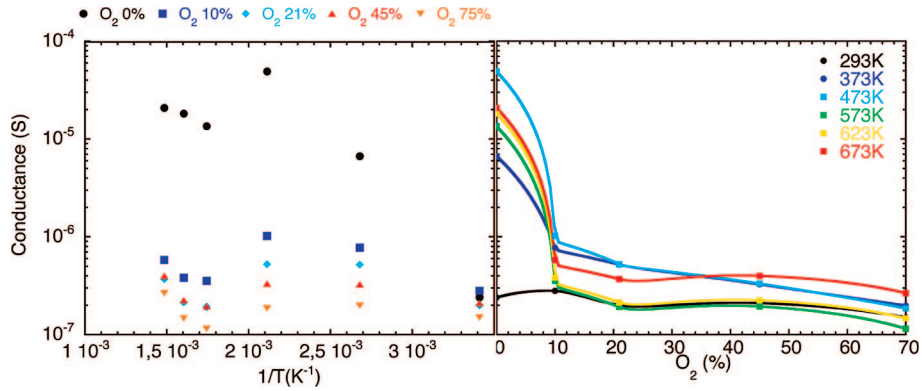

Figure 2. Electrical conductance data of SnO_2 nanocrystals as a function of $1/T$ for various oxygen concentrations (left), and the same data plotted as a function of the oxygen concentrations (right).

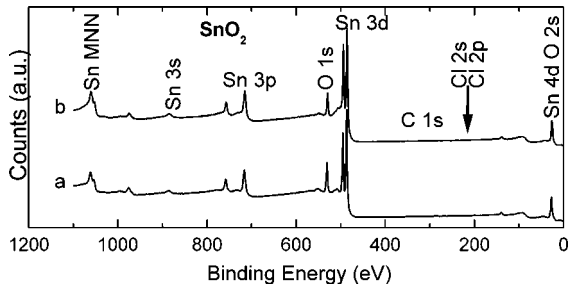

Figure 3. XPS survey spectra of SnO_2 nanocrystals heat-treated at 500 °C, measured on (a) the as-prepared sample and (b) after sputtering with Ar^{3+} ions. The spectra have been vertically shifted for clarity.

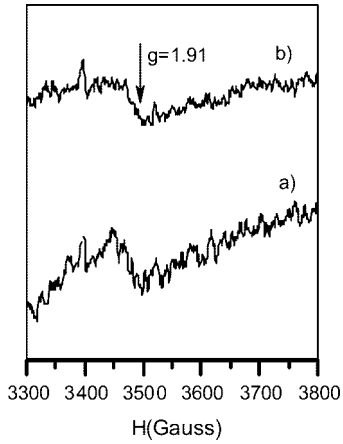

Figure 4. EPR spectra measured on SnO_2 nanocrystals under the following conditions: (a) after annealing in air at 400 °C; (b) after treatment with CO(600 ppm)/Ar at 400 °C.

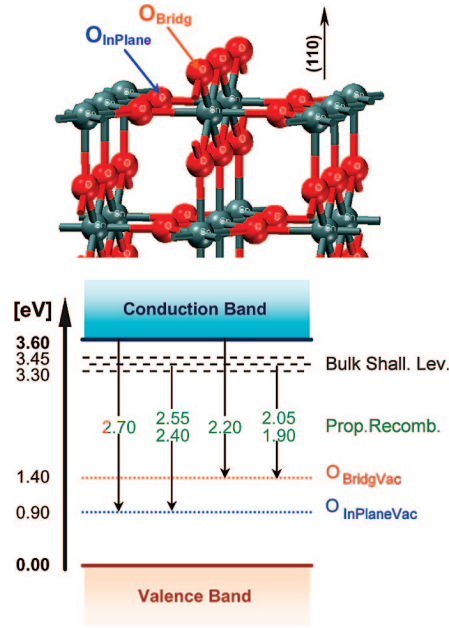

Figure 5. (Top) Slab model of the SnO_2—cassiterite (110) surface. Bridging and in-plane oxygen sites are identified. (Bottom) Schematic representation of the intragap levels of SnO_2 corresponding to bulk shallow levels and oxygen vacancies at the surface. For clarity, energy zero has been set at the top of the valence band (VBM). Recombinations compatible with the CL spectra are shown.

processing.[17] We then applied the model to our samples. At the top of Figure 6, the CL spectra of the SnO_2 nanocrystals dried at 80 °C are shown, together with the fitting of the band by the four components previously described. In the nanocrystals heat-treated at 500 °C, the CL signal shape undergoes modifications due to the relative intensity changes of the single components, in particular the components I and II grow in intensity with respect to the components III and IV (Figure 6, bottom panel). According to the previous model, the change corresponds to an increase in the radiative recombination involving the $O_{BridgVac}$-related state. Thus, it appears that both types of surface oxygen vacancies are present in the as prepared (dried at 80 °C) sample and that the thermal treatment at 500 °C mainly produced $O_{BridgVac}$.

Ab initio thermodynamics[19] helped us clarify why the generation of $O_{BridgVac}$ is favored, by discussing the energetic requirements for the oxygen vacancy production at 500 °C in synthetic air. We followed the methodology described by Reuter and Scheffler[26] to elucidate the most favorable surface configuration in equilibrium with the oxygen content in air at a given pressure and temperature (or, equivalently, a given oxygen chemical potential μ_O). This methodology consists of applying a minimum energy criterion to the surface energy versus μ_O plots of every relevant surface configuration. In Figure 7 we report these plots for the stoichiometric, the O_{Bridg} reduced and $O_{InPlane}$ reduced surface terminations. The most stable surface configuration after heat treatment at 500 °C, and therefore the most likely, corresponds to a reduced surface due to $O_{BridgVac}$ generation. This prediction agrees with previous theoretical[27,28] and experimental work[29] in which $O_{BridgVac}$ generation was observed at temperatures ranging from 225 to 525 °C.

(e) Summary: a Strongly Reduced SnO_2 Surface with Well Defined Defects Distribution. The results presented in the previous sections concur to define the picture of a strongly reduced nanocrystal surface, with an oxygen substoichiometry dictated by the heat treatment step. The substoichiometry is

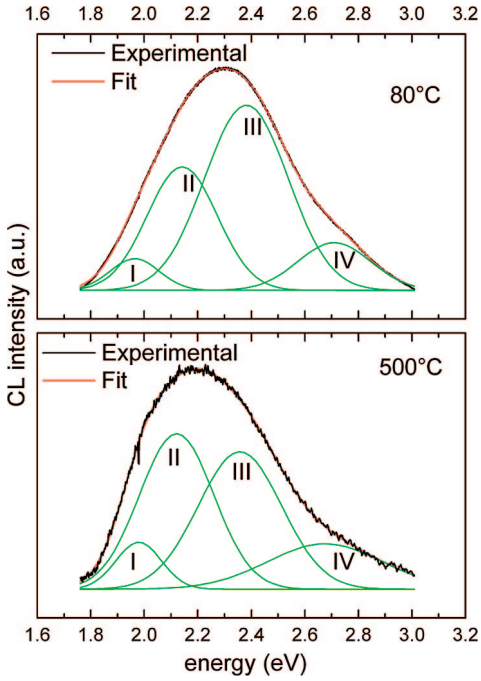

Figure 6. CL spectra measured on SnO_2 nanocrystals heated at the indicated temperatures, together with the fitting (green bands) with the components described in the text.

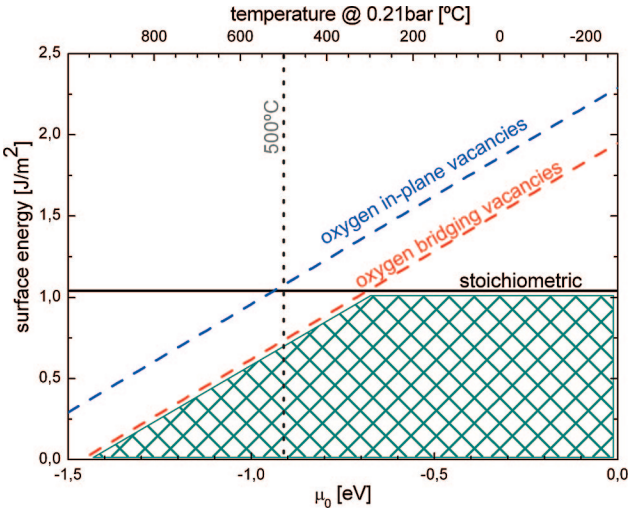

Figure 7. Surface free energies for three different terminations of the $SnO_2(110)$ surface as a function of the oxygen chemical potential. The top axis shows the corresponding O_2 gas temperature for synthetic air equivalent conditions (i.e., oxygen partial pressure of ~0.21 bar). Shaded area is limited by the minimum energy configuration at different air temperatures. At 500 °C (the experimental thermal treatment temperature) the most energetically favorable configuration is the surface reduction by generation of surface bridging vacancies ($O_{BridgVac}$).

directly indicated by the XPS results, while EPR data show that the surface reduction has occurred to a remarkable extent, so that further reduction is not allowed. The electrical conductance data (Figure 2) show that the reaction of gaseous oxygen with the nanocrystal surface is extremely favored. We have already mentioned that the data imply a prevalence of oxygen ionosorption. Now, this result can be interpreted as an indication of the adsorbing activity of the oxygen vacancies. In particular, it is known that bridging oxygen vacancies can strongly bond oxygen species.[30] Finally, the CL data allowed a careful identification of the involved oxygen vacancies, present as both bridging and in plane species. The former are generated in the heat-treated nanocrystals, for thermodynamic reasons.

Discussion

The main question to answer is whether it is possible to find a correlation between the properties shown in sections 1 and 2, related to NO_2 sensing, and the surface chemical state. The possible link is suggested by the NO_2 sensing mechanism reported in the introduction, which implies NO_2 adsorption and subsequent increase of the electrical resistance. Because the oxygen vacancies make the SnO_2 surfaces strongly amenable to oxygen ionosorption, it is necessary to ask whether the oxygen vacancies may influence also the NO_2 adsorption and what is the effect of the adsorption onto the charge distribution in the nanocrystals. This task was accomplished by DFT simulation of the NO_2 adsorption onto SnO_2 surfaces in the presence of variable concentration of oxygen vacancies.

First of all, it is known from previous work on the simulation of temperature-programmed desorption (TPD) data[19,20] that NO_2 tends to adsorb onto $SnO_2(110)$ $O_{InPlane}$ and $O_{BridgVac}$ sites. The former site was found to be related to the low temperature TPD band (from 50 to 300 °C) while the latter site was responsible for the TPD signal from 350 to 500 °C. The very large responses to NO_2 at room temperature or 100 °C, reported in the section 1 of the Results, would then indicate that the sensing-promoting sites are the $O_{InPlane}$ vacancies. On the other hand, we have shown in the previous sections that the heat treatment at 500 °C stimulates the generation of vacancies related to O_{Bridg} sites. In order to obtain further insight into the sensing performances, it is necessary to solve this apparent contradiction. Hence, we studied the influence of the reduction percentage on the surface−adsorbate interaction from first principles. For the most relevant adsorption configurations reported previously,[19,20] and detailed in the Supporting Information, we calculated both the strength of the adsorption (the adsorption energy E_{ads}) and the resulting charge transfer ($\Delta q(NO_2)$) between the NO_2 molecule and the substrate. To model the changes in the surface reduction percentage, we removed from the atomistic models an increasing number of O_{Bridg}. It can be shown that only about a 10% of the available adsorption sites are effectively occupied by NO_2[31] (this is justified by the Weisz limitation,[32] which takes into account the electrostatic repulsion forces among the adsorbed species). To reach equivalent occupancies, we used a 3 × 3 supercell. With this model, occupancies of 11% onto $O_{BridgVac}$ were studied. At every reduction percentage all non-symmetry-equivalent vacancy distributions around the adsorbate were considered.

In Figure 4 we report the computed E_{ads} and $\Delta q(NO_2)$ for adsorption at lower temperatures (NO_2 onto an $O_{InPlane}$ site). Exothermic adsorption energies are assumed as negative E_{ads} values, and charge transfers refer to the adsorbate (positive $\Delta q(NO_2)$ means electron capture by the NO_2 molecule).

Thus, more negative E_{ads} energy means stronger adsorption, and a higher $\Delta q(NO_2)$ implies a bigger charge captured by NO_2. The calculations predict that reduction slightly favors the adsorption (maximum of a 20% in energy) and *almost doubles* the charge transfer to the adsorbate. From the point of view of the gas response, the effectiveness of the sensing sites is determined by (1) the continuous adsorption and desorption processes (which are determined by the analyte concentration, the energetics of the interaction, and the working temperature), and (2) the net charge exchange between the metal oxide and adsorbate (which determines the electrical response). Our results demonstrate that the surface reduction influences both the energy exchange and the charge transfer between surface and analyte.

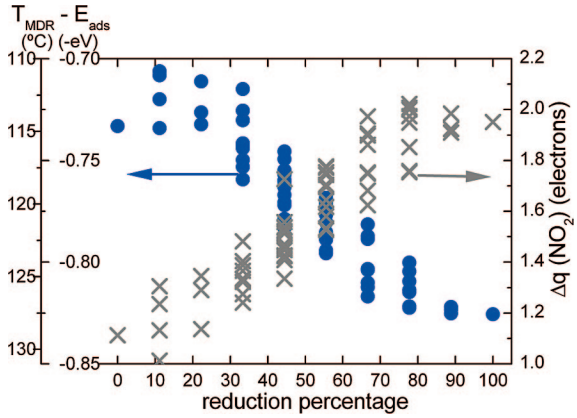

Figure 8. Influence of the reduction percentage (only due to $O_{BrigVac}$ generation) on the energetics and charge transfers of NO_2 adsorption onto an $O_{InPlane}$ site[19] at the SnO_2(110) surface. The adsorption energy (E_{ads}) and the corresponding maximum desorption rate temperature (T_{MDR}) are represented in the left axis. T_{MDR} were calculated by solving the Redhead[33,34] equation with the experimental conditions reported elsewhere.[35] The charge transferred to the adsorbate $\Delta q(NO_2)$ was estimated by the usual Mulliken's population analysis of the molecule atoms before and after the adsorption.

Concretely, the effect of removing O_{Bridg} atoms from the SnO_2 (110) surface on the NO_2 adsorption onto $O_{InPlane}$ sites is a slight modification of the desorption temperatures and a strong increase of the charge trapped by this adsorbate. A strong influence on the sensor performance by the $O_{BridgVac}$ generation (by thermally treating the SnO_2 nanoparticles) then appears. For completeness, in the Supporting Information a plot similar to Figure 8 is reported but related to the adsorption onto the $O_{BridgVac}$ sites. Effects similar to those observed for the $O_{InPlane}$ sites are observed, despite the $O_{BridgVac}$ sites that are active at higher operating temperatures, as mentioned above.

Comparison with Other Work. The importance of the surface oxygen vacancies is further highlighted by comparison with other work. The computational approach to the understanding of the adsorption and gas-sensing properties of SnO_2 is well-known,[36] and recent results in the case of NO_2 sensing have been published.[15] In such work, the authors have extensively studied the adsorption of NO_2 onto various sites and in different configurations. The main results were the following: on *defect-free* surfaces, current drop by NO_2 adsorption is expected, due to NO_2 interaction with surface Sn atoms, and in particular upon formation of a bridging nitrate groups. When oxygen vacancies are introduced in the model, an enhanced conductance drop is expected upon interaction of oxygen with the *oxygen vacancies* and the neighboring Sn atoms, and the same behavior is expected for NO_2. In this work, we reported, both from an experimental and computational point of view, a significant current drop upon interaction of the SnO_2 nanocrystals with NO_2. Moreover, in Figure 2 a similar, large conductance drop is reported for interaction of the SnO_2 sample with oxygen. The observed trends are in agreement with results from ref 15 (where the authors simulate vacancies on (10-1) surfaces). This comparison shows that a careful computational approach is fundamental in unraveling the complex sensing phenomena. On the other hand, the distance of the computational models from the real operating conditions requires the simulation work to be constantly backed up by well-defined experimental data, in order to have a constant check of how much realistic the computational results can be.

Conclusions

The NO_2 sensing properties of SnO_2 nanocrystals have been investigated by comparing the experimental surface chemistry with the DFT modeling of the adsorption properties. It was found that the heat-treatment conditions (500 °C in air) favored the formation of surface oxygen vacancies, as demonstrated by electrical, XPS, EPR, and cathodoluminescence (CL) measurements and the CL-related DFT modeling. In particular, an increase of the bridging oxygen vacancies was observed, and the surface reduction effect on the NO_2 adsorption was studied by DFT modeling. It appeared that the interaction of NO_2 with the surface occurs through the oxygen vacancy sites, and that the presence of bridging oxygen vacancies strongly enhances the charge transfer from the surface to NO_2. Thus the achievement of remarkable gas-sensing properties was concluded to be not only a function of the small oxide grain but also of suitable surface-reception properties, which in the case of NO_2 we have related to oxygen vacancies.

Acknowledgment. This work was supported by the European Union in the frame of the project NANOS4 (Grant NMP4-CT-2003-001528) and by the Spanish Ministry of Education (MEC) through the projects n-MOSEN (MAT2007-66741-C02-01), NANOAMPER (CIT-030000-2007-36), and MAGASENS (NAN2004-09380-C04-01). J.D.P. is indebted to the MEC for the FPU grant. The computer resources, technical expertise, and assistance provided by the Barcelona Supercomputing Center - Centro Nacional de Supercomputación and the Supercomputing Center of Catalonia are gratefully acknowledged.

Supporting Information Available: Plots of the relevant adsorption configurations for NO_2 and plot of the influence of the reduction percentage (only due to OBrigVac generation) on the energetics and change transfers of NO_2 adsorption onto an OBrigVac site. This material is available free of charge via the Internet at http://pubs.acs.org.

References and Notes

(1) (a) Chaonan Xu, C.; Tamaki, J.; Miura, N.; Yamazoe, N. *Sens. Actuators B* **1991**, *3*, 147. (b) Yamazoe, N. *Sens. Actuators B* **1991**, *5*, 7.

(2) (a) Vuong, D. D.; Sakai, G.; Shimanoe, K.; Yamazoe, N. *Sens. Actuators B* **2005**, *105*, 437. (b) Ruiz, A. M.; Cornet, A.; Shimanoe, K.; Morante, J. R.; Yamazoe, N. *Sens. Actuators B* **2005**, *108*, 34. (c) McCue, J. T.; Ying, J. Y. *Chem. Mater.* **2007**, *19*, 1009. (d) Chiu, H.-C.; Yeh, C.-S. *J. Phys. Chem. C* **2007**, *111*, 7256. (e) Erades, L.; Grandjean, D.; Nayral, C.; Soulantica, K.; Chaudret, B.; Menini, P.; Parret, F.; Maisonnat, A. *New J. Chem.* **2006**, *7*, 1026.

(3) (a) Comini, E. *Anal. Chim. Acta* **2006**, *568*, 28; this reference includes an exhaustive list of 1-D based gas sensors. (b) Kolmakov, A.; Zhang, Y.; Cheng, G.; Moskovits, M. *Annu. Rev. Mater. Res.* **2004**, *34*, 151. (c) McAlpine, M. C.; Ahmad, H.; Wang, D.; Heath, J. H. *Nat. Mater.* **2007**, *6*, 379. (d) Polleux, J.; Gurlo, A.; Barsan, N.; Weimar, U.; Antonietti, M.; Niederberger, M. *Angew. Chem., Int. Ed.* **2006**, *45*, 261. (e) Rout, C. S.; Govindaraj, A.; Rao, C. N. R. *J. Mater. Chem.* **2006**, *16*, 3936. (f) Du, N.; Zhang, H.; Chen, B.; Ma, X.; Liu, Z.; Wu, J.; Yang, D. *Adv. Mater.* **2007**, *19*, 1641.

(4) Epifani, M.; Díaz, R.; Arbiol, J.; Comini, E.; Sergent, N.; Pagnier, T.; Siciliano, P.; Faglia, G.; Morante, J. R. *Adv. Funct. Mater.* **2006**, *16*, 1488.

(5) (a) Epifani, M.; Comini, E.; Diaz, R.; Arbiol, J.; Siciliano, P.; Sberveglieri, G.; Morante, J. R. *Sens. Actuators B* **2006**, *118*, 105. (b) Epifani, M.; Diaz, R.; Arbiol, J.; Comini, E.; Sergent, N.; Pagnier, T.; Siciliano, P.; Faglia, G.; Morante, J. R. *Sens. Actuators B* **2007**, *126*, 163. (c) Epifani, M.; Comini, E.; Arbiol, J.; Pellicer, E.; Siciliano, P.; Faglia, G.; Morante, J. R. *J. Phys. Chem. C* **2007**, *111*, 13967. (d) Epifani, M.; Arbiol, J.; Pellicer, E.; Comini, E.; Siciliano, P.; Faglia, G.; Morante, J. R. *Cryst. Growth Des.* **2008**, *8*, 1774.

(6) Yamazoe, N.; Shimanoe, K. *Sens. Actuators B* **2008**, *128*, 566.

(7) Hohenberg, P.; Kohn, W. *Phys. Rev.* **1964**, *136*, B864.

(8) Kohn, W.; Sham, L. J. *Phys. Rev.* **1965**, *140*, A1133.

(9) Ordejón, P.; Artacho, E.; Soler, J. M. *Phys. Rev. B* **1996**, *53*, R10441.

(10) Soler, J. M.; Artacho, E.; Gale, J. D.; García, A.; Junquera, J.; Ordejón, P.; Sánchez-Portal, D. *J. Phys.: Condens. Matter* **2002**, *14*, 2745.

(11) Perdew, J. P.; Burke, K.; Ernzerhof, M. *Phys. Rev. Lett.* **1996**, *77*, 3865.

(12) Troullier, N.; Martins, J. L. *Phys. Rev. B* **1991**, *43*, 1993.
(13) Bolzan, A. A.; Fong, C.; Kennedy, B. J.; Howard, C. J. *Acta Crystallogr., Sect. B: Struct. Sci.* **1997**, *53*, 373.
(14) Oviedo, J.; Gillan, M. J. *Surf. Sci.* **2002**, *513*, 26.
(15) Maiti, A.; Rodriguez, J. A.; Law, M.; Kung, P.; McKinney, J. R.; Yang, P. *Nano Lett.* **2003**, *3*, 1025.
(16) Batzill, M.; Katsiev, K.; Burst, J. M.; Diebold, U.; Chaka, A. M.; Delley, B. *Phys. Rev. B* **2005**, *72*, 165414.
(17) Prades, J. D.; Arbiol, J.; Cirera, A.; Morante, J. R.; Avella, M.; Zanotti, L.; Comini, E.; Faglia, G.; Sberveglieri, G. *Sens. Actuators B* **2007**, *126*, 6.
(18) Prades, J. D.; Cirera, A.; Morante, J. R.; Cornet, A. *Thin Solid Films* **2007**, *515*, 8670.
(19) Prades, J. D.; Cirera, A.; Morante, J. R. *J. Electrochem. Soc.* **2007**, *154*, H675.
(20) Prades, J. D.; Cirera, A.; Morante, J. R.; Pruneda, J. M.; Ordejón, P. *Sens. Actuators B* **2007**, *126*, 62.
(21) Monkhorst, H.; Pack, J. *Phys. Rev. B* **1976**, *13*, 5188.
(22) Boys, S. F.; Bernardi, F. F. *Mol. Phys.* **1970**, *19*, 553.
(23) Barsan, N.; Schweizer-Berberich, M.; Gopel, W. *Fresenius J. Anal. Chem* **1999**, *365*, 287, and references therein.
(24) (a) Canevali, C.; Chiodini, N.; Di Nola, P.; Morazzoni, F.; Scotti, R.; Bianchi, C. L. *J. Mater. Chem* **1997**, *7*, 997. (b) Canevali, C.; Chiodini, N.; Morazzoni, F.; Scotti, R. *J. Mater. Chem.* **2000**, *10*, 773. (c) Armelao, L.; Barreca, D.; Bontempi, E.; Morazzoni, F.; Canevali, C.; Depero, L. E.; Mari, C. M.; Ruffo, R.; Scotti, R.; Tondello, E. *Appl. Magn. Reson.* **2002**, *22*, 89.
(25) (a) Huang, M. H.; Wu, Y.; Feick, H.; Tran, N.; Weber, E.; Yang, P. *Adv. Mater.* **2001**, *13*, 113. (b) Yao, B. D.; Chan, Y. F.; Wang, N. *Appl. Phys. Lett.* **2002**, *81*, 757.
(26) Reuter, K.; Scheffler, M. *Phys. Rev. B* **2002**, *65*, 035406.
(27) Oviedo, J.; Gillan, M. J. *Surf. Sci.* **2000**, *467*, 35.
(28) Duan, Y. *Phys. Rev. B* **2008**, *77*, 045332.
(29) (a) Cox, D. F.; Fryberger, T. B.; Semancik, S. *Phys. Rev. B* **1988**, *38*, 2072. (b) Cox, D. F.; Fryberger, T. B.; Semancik, S. *Surf. Sci.* **1990**, *227*, L105.
(30) Batzill, M.; Diebold, U. *Prog. Surf. Sci.* **2005**, *79*, 47. in particular pp. 122−124.
(31) Hernandez-Ramirez, F.; Prades, J. D.; Tarancon, A.; Barth, S.; Casals, A.; Jimenez-Diaz, R.; Pellicer, E.; Rodriguez, J.; Morante, J. R.; Juli, M. A.; Mathur, S.; Romano-Rodriguez, A. *Adv. Funct. Mater.* **2008**, *18*, 2990. (, DOI: 10-1002/adfm.200701191).
(32) Weisz, P. B. *J. Chem. Phys.* **1953**, *21*, 1531.
(33) Desjonquères, M. C.; Spanjaard, D. *Concepts in Surface Physics*, 2nd ed.; Springer: Berlin, 1996.
(34) Zhdanov, V. P.; Kasemo, B. *Surf. Sci.* **1998**, *415*, 403.
(35) Leblanc, E.; Perier-Camby, L.; Thomas, G.; Gibert, R.; Primet, M.; Gelin, P. *Sens. Actuators B* **2000**, *62*, 67.
(36) Batzill, M.; Diebold, U. *Prog. Surf. Sci.* **2005**, *79*, 47, in particular pp 120−132 and references therein.

JP804916G